01 Mar 2014

Computational Study of the Rovibrational Spectrum of CO_2-CS_2

James Corgan Brown

Xiao-Gang Wang

Tucker Carrington Jr.

Garry S. Grubbs
Missouri University of Science and Technology, grubbsg@mst.edu

et. al. For a complete list of authors, see https://scholarsmine.mst.edu/chem_facwork/2178

Computational study of the rovibrational spectrum of CO_2–CS_2

James Brown,[1,a)] Xiao-Gang Wang,[2,b)] Tucker Carrington, Jr.,[2,c)] G. S. Grubbs II,[3,d)] and Richard Dawes[3,e)]
[1]*Department of Physics, Engineering Physics, and Astronomy, Queen's University, Kingston, Ontario K7L 3N6, Canada*
[2]*Chemistry Department, Queen's University, Kingston, Ontario K7L 3N6, Canada*
[3]*Department of Chemistry, Missouri University of Science and Technology, Rolla, Missouri 65409-0010, USA*

(Received 23 January 2014; accepted 24 February 2014; published online 18 March 2014)

A new intermolecular potential energy surface, rovibrational transition frequencies, and line strengths are computed for CO_2–CS_2. The potential is made by fitting energies obtained from explicitly correlated coupled-cluster calculations using an interpolating moving least squares method. The rovibrational Schrödinger equation is solved with a symmetry-adapted Lanczos algorithm and an uncoupled product basis set. All four intermolecular coordinates are included in the calculation. In agreement with previous experiments, the global minimum of the potential energy surface (PES) is cross shaped. The PES also has slipped-parallel minima. Rovibrational wavefunctions are localized in the cross minima and the slipped-parallel minima. Vibrational parent analysis was used to assign vibrational labels to rovibrational states. Tunneling occurs between the two cross minima. Because more than one symmetry operation interconverts the two wells, the symmetry (−oo) of the upper component of the tunneling doublet is different from the symmetry (−ee) of the tunneling coordinate. This unusual situation is due to the multidimensional nature of the double well tunneling. For the cross ground vibrational state, calculated rotational constants differ from their experimental counterparts by less than 0.0001 cm^{-1}. Most rovibrational states were found to be incompatible with the standard effective rotational Hamiltonian often used to fit spectra. This appears to be due to coupling between internal and overall rotation of the dimer. A simple 2D model accounting for internal rotation was used for two cross-shaped fundamentals to obtain good fits. [http://dx.doi.org/10.1063/1.4867792]

I. INTRODUCTION

Large amplitude motion has intrigued experimentalists and theorists for many years.[1–5] It is important because it reveals large regions of a potential energy surface (PES), and is a precursor to motion that breaks and makes chemical bonds. Van der Waals (VdW) clusters undergo large amplitude motion even at low energies.[6–10] Theoretical/computational tools that make it possible to calculate rovibrational spectra of Van der Waals clusters composed of two molecules are well established.[11–15] For these clusters, it is a good approximation to use an adiabatic approximation and neglect coupling between intra- and inter-molecular coordinates. With this approximation a cluster made up of two linear molecules has 4 vibrational and 3 rotational coordinates and is easily amenable to product basis Lanczos methods. Owing to the complexity of the dynamics and the large amplitude of the vibrations, it is necessary to use variational numerical methods to compute a spectrum. To understand the spectrum of a molecule undergoing large amplitude motion, it is also necessary to construct a PES by computing *ab initio* points and fitting them to a functional form.[16–25] Simple Taylor series representations are inadequate. *Ab initio* and fitting methods are now good enough that one can build extremely accurate PESs for clusters with 4 inter-molecular coordinates.[14,26,27] We have previously computed spectra of Van der Waals clusters with two linear monomers.[14,26,27] In all of these clusters, there are several low-lying planar minima connected by planar paths. CO_2–CS_2 is different because experimentally its structure is non-planar. In this paper, we build a new PES for this cluster and by computing energy levels and wavefunctions show that out-of-plane motion is important. The two (linear) monomers rotate with respect to each other and due to this internal rotation, all semi-rigid models work poorly. For $(N_2O)_2$,[26] $(CO)_2$, and $(OCS)_2$, we were able to associate rovibrational levels with vibrational states and fit them to a standard energy level expression in terms of rotational and centrifugal distortion constants.[28] For CO_2–CS_2, this works for the ground vibrational state, but not for others. In general, the standard fit fails when rovibrational coupling is too strong. For CO_2–CS_2, it fails because of strong coupling between the internal rotation and the overall rotation. When it fails, rotational constants become meaningless.

The PESs of VdW clusters often have several minima. Nonetheless, it may be true that wavefunctions are localized enough that experimentalists are able to determine the shape of the most stable isomer. The global minimum of linear-linear VdW clusters is sometimes linear, sometimes T-shaped, and sometimes has a slipped parallel shape.

a)Electronic mail: 9jhb3@queensu.ca
b)Electronic mail: xgwang.dalian@gmail.com
c)Electronic mail: Tucker.Carrington@queensu.ca
d)Electronic mail: grubbsg@mst.edu
e)Electronic mail: dawesr@mst.edu

CO_2–N_2O, CO_2–acetylene, CO_2–CO_2, and CO_2–OCS all have slipped parallel global minima. CO_2–HCl,[29,30] CO_2–Br_2,[31] and CO_2–HF[30,32] have linear global minima. CO_2–HBr has a T-shaped global minimum. CO_2–HCN has two deep minima, one nearly linear[33] and one T-shaped.[33,34] According to the first infrared study of CO_2–CS_2, it is cross-shaped, i.e., nonplanar and not linear, T-shaped, or slipped parallel.[35] Other clusters have also been shown to have non-planar minima. CO_2–OCS has not only a slipped parallel global minimum but also a stable cross-shaped structure.[36] CO_2 clusters with nonlinear monomers, such as CO_2–H_2S[37] and CO_2–SO_2[38] have non-planar minima. Experimental determination of the shape of the global minimum is only possible if rovibrational coupling is weak enough that spectra can be fit to a traditional expansion in powers of rotational quantum numbers. We predict that this will only be partially successful for CO_2–CS_2. We confirm the conclusion of Dutton *et al.*[35] that the cross-shaped minimum of CO_2–CS_2 is the deepest, but find a slipped parallel structure that is very close in energy.

II. THE POTENTIAL ENERGY SURFACE

The coordinates used to define the PES are r_0, r_1, r_2, θ_1, θ_2, ϕ_2, and are shown in Fig. 1. The $\vec{r}_0$ vector points from the center-of-mass of the CO_2 monomer to the center-of-mass of the CS_2 monomer. The $\vec{r}_1$ and $\vec{r}_2$ vectors point along the monomers. θ_1 and θ_2 define the angle between $\vec{r}_0$, and $\vec{r}_1$ and $\vec{r}_2$, respectively. ϕ_2 is defined as the dihedral angle between the two normal vectors $\vec{r}_0 \times \vec{r}_1$ and $\vec{r}_0 \times \vec{r}_2$. r_1 and r_2 are fixed at values consistent with rotational constants of CO_2 and CS_2. The PES depends only on the intermolecular coordinates.

A. Interpolating moving least squares (IMLS) PES fitting

The four-dimensional (4D) intermolecular CO_2–CS_2 potential is made from 1667 symmetry-unique high-level *ab initio* energy points, and is represented analytically by the IMLS method using a weight function to interpolate between local fitting basis expansions.[23,39] The CO_2–CS_2 system is similar to the previously studied $(NNO)_2$,[14] $(OCS)_2$,[27] and $(CO)_2$[40] systems from a fitting standpoint (weakly interacting rigid linear monomers) but has some differences with respect to symmetry. Whereas the $(N_2O)_2$, $(OCS)_2$, and $(CO)_2$ systems are composed of identical monomers and thus have monomer exchange symmetry, CO_2–CS_2 lacks that exchange symmetry, but each monomer is symmetric with respect to exchange of the two end-atom nuclei. The fitting basis (mentioned below) can be adapted to treat these symmetries by placing simple constraints on the basis indices. However, when the basis is used interpolatively (as we do here), imposing symmetry is slightly more complicated since, for example (due to the chain-rule) the gradient is due to both the gradient of the basis functions and the changing weights. A simple way to obtain correct behavior is to add the symmetry partners for each symmetry-unique *ab initio* data point to the fitting set. There is no additional cost in terms of electronic structure calculations and for cases of relatively low permutation symmetry (a factor of four is obtained for CO_2–CS_2) the fitting set does not become too unwieldy. For systems with very high permutation symmetry, development of a permutation invariant basis would be preferred.[22] The automated procedure that was developed to construct 4D PESs for $(NNO)_2$, $(OCS)_2$, and $(CO)_2$ and has been described in detail previously[14,27] was employed here. The same inter-monomer coordinates and a fitting basis of 301 functions composed of products of radial functions with spherical harmonics type bend functions were used. The same distance metric, interpolative weight function, and singular value decomposition-based dynamic conditioning procedure were also used. For CO_2–CS_2, the range of inter-monomer center-of-mass distances was r_0 = [2.8, 15.0] Å, while the fitted energy range included all stable isomers (the global minimum has a well depth of 542 cm^{-1}), but was restricted to 6.0 kcal/mol (2100 cm^{-1}) above the separated monomers asymptote. As was done previously, to avoid computing and discarding costly high-level *ab initio* data in highly repulsive regions, an initial low-level guide surface was constructed. For the low-level surface, a set of 1200 symmetry unique points were distributed according to a Sobol sequence[41] subject to an exponential r_0-dependent bias that favors points at r_0 = 2.8 Å over points at r_0 = 15.0 Å by a factor of 20 (making the short-range repulsive region much more densely sampled). As before, the guide surface was fit using the same IMLS scheme as the final high-level PES, but with a smaller fitting basis of only 40 functions per local expansion. For the high-level PES, 1000 initial seed points were distributed the same way according to the exponentially radially biased Sobol sequence, but with high-energy regions excluded by the lower level guide surface. Starting from the 1000 seed points, sets of 48 automatically determined points were added in each of a series of iterations until the estimated RMS fitting error was reduced to below 0.8 cm^{-1}. The accuracy of the final PES was tested using a random set of 288 points, confirming the estimated sub-wavenumber accuracy. The PES generation algorithm and fitting error estimate method have been described previously, and were applied here with the entire coordinate and energy range fit without bias, in an automated fashion. The PES generation algorithm was terminated and finalized for use in this case with a total of 1667 symmetry unique points. This is similar to the 1757 points used to fit the $(NNO)_2$ PES, and the final fitting error is slightly lower.

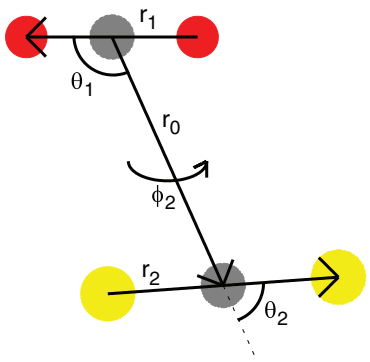

FIG. 1. A schematic of the coordinates used for rovibrational calculations of CO_2–CS_2. O is red, C is grey, and S is yellow.

B. Electronic structure theory

The monomers were held rigid in a collinear arrangement with internuclear bond distances fixed at values obtained from experimental rotational constants: $R_{OC} = 1.16209$ and $R_{CS} = 1.5526$ Å.

Since the PES represents the VdW interaction of two closed shell species, single reference coupled-cluster based methods were chosen. The MOLPRO[42] electronic structure package was used for all of the calculations reported here. For $(NNO)_2$ and $(CO)_2$, we have previously reported extensive benchmarking of various complete basis set (CBS) extrapolations of coupled cluster with singles, doubles and perturbative triple excitations (CCSD(T)) energies computed with correlation-consistent basis sets at a series of zeta levels. For those systems, extrapolations of standard CCSD(T) energies were compared with results obtained with explicitly correlated F12 methods. We find that for the closed-shell VdW systems considered, the explicitly correlated F12b method converges the singles and doubles contributions to electron correlation very close to the CBS limit values, if a basis set at least as large as VTZ-F12 is used. Thus, if the triples contribution is small, we favor using the CCSD(T)-F12b method directly without CBS extrapolation. The perturbative triples (T) contribution is not directly included in the F12b explicit correlation formalism and so if that contribution is large, then basis set extrapolation may still be necessary (this is the case for $(CO)_2$). The (T) contribution is not particularly large in CO_2–CS_2, so for the final high-level PES, the explicitly correlated CCSD(T)-F12b method was used with Peterson's specialized VTZ-F12 basis set (without CBS extrapolation).[43] The low-level guide surface was fit to data at the CCSD(T)-F12a/VDZ-F12 level. The T_1-diagnostic was monitored and found to be roughly 0.019 for all geometries in the high-level data set.

III. PROPERTIES OF THE PES

A. Minima

The CO_2–CS_2 PES surface has 10 wells: 4 symmetrically equivalent slipped-parallel wells, 2 symmetrically equivalent cross-shaped wells, and 4 symmetrically equivalent bent wells. The 4 symmetrically equivalent slipped-parallel wells correspond to the polar and nonpolar minima and saddle points of $(N_2O)_2$ and $(OCS)_2$. $(OCS)_2$ also has bent and cross-shaped wells similar to those we find for CO_2–CS_2. The geometries and energies, relative to the dissociation energy of the minima, are given in Table I. The cross-shaped wells are only 2.64 cm^{-1} deeper than the slipped-parallel wells. The slipped-parallel structure is not exactly parallel as $\theta_1 + \theta_2 \neq 180^\circ$. The bent wells are significantly higher and shallower than the other wells. Schematics of the cross-shaped and slipped-parallel structures are given in Fig. 2. The only experimentally determined structure is cross-shaped.[35] The experimental value of r_0 is 6.410 bohr, which is larger than the equilibrium value in Table I by 0.118 bohr. The experimental value is larger due to vibrational averaging.

TABLE I. The local minima of the CO_2–CS_2 PES.

Coordinate	Slipped parallel	Cross shaped	Bent
r_0 (Bohr)	6.946	6.292	11.180
θ_1 (deg)	114.103	90.000	19.463
θ_2 (deg)	70.021	90.000	8.410
ϕ_2 (deg)	180.00	90.000	180.00
E (cm^{-1})	− 539.03	− 541.67	− 314.94
$E - E_0$ (cm^{-1})	2.64	0.00	226.73

B. Paths between minima

Fig. 3 shows a 2D contour plot of the PES made by constraining CO_2–CS_2 to be planar and choosing r_0 to minimize the energy for each pair of angles θ_1, θ_2. The potential is plotted as a function of the extended angles defined in Refs. 26 and 40. See Figure 2 of Ref. 40 for the complete definition of the extended angles. $\phi_2 = \pi$ in the squares with corners at $[-\pi, -\pi]$ and $[+\pi, +\pi]$. The wells are labeled by SP for slipped parallel and B for bent. Due to the use of extended coordinates every molecular shape corresponds to two points on the potential.

The low-lying planar paths are rather different than those of other dimers we have studied for which interconversion of isomers proceeds via a disrotatory cycle.[14,26,44] For CO_2–CS_2, the barrier between SP7 and SP3, over a T-shaped transition state, is large. The low-lying planar path is most easily visualized by thinking of the bottom half of Fig. 3 as being the physical potential and of points on the top half as being obtained from points in the bottom half by rotation of the molecule. For example, the SP3 well is a copy of the SP6 well. The barrier between SP7 (SP6) and SP1 (SP4) is about 155 cm^{-1}. At the top of the barrier(s) the two monomers are perpendicular to the inter-monomer axis. These two sets of two wells are separated by a barrier between SP1 and SP6 of about 255 cm^{-1}. The structure at the top of this barrier is T-shaped. The barrier between SP7 and B2 is about 240 cm^{-1}. The bent minima are less than 10 cm^{-1} below the energy of the linear configuration at $\tilde{\theta}_1 = \tilde{\theta}_2 = 0^\circ$. The bent minima are about 15 cm^{-1} below the barrier to a SP minimum. Because the bent wells are high and very shallow, no wavefunctions are localized in these wells.

A more important path linking SP1 and SP4 or SP7 and SP6 is out-of-plane. Fig. 4 shows the out-of-plane ϕ_2 path

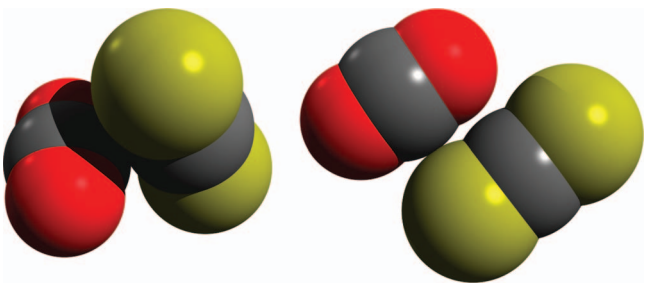

FIG. 2. The cross-shaped (left) and slipped-parallel (right) isomers of the CO_2–CS_2 dimer on the PES with Van der Waals radii of O (red), C (grey), and S (yellow) of 1.4, 1.5, and 1.85 Å (respectively).

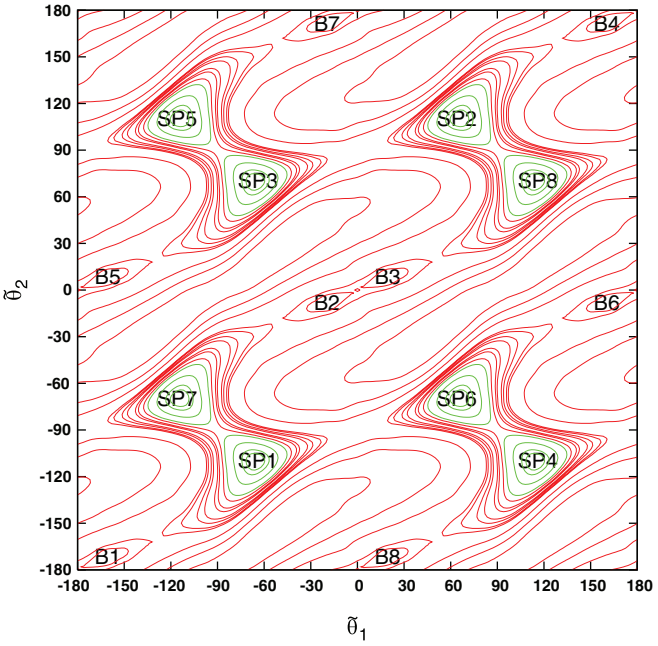

FIG. 3. Potential as a function of extended angles $(\tilde{\theta_1}, \tilde{\theta_2})$ obtained by minimizing with respect to r_0. The contours correspond to energies of −100, −150, −200, −250, −300, −307.5, −320, −330, −350, −360, −380, −400, −450, −500, and −520 cm^{-1}. Green contours are those below −380 cm^{-1}.

connecting SP1 to SP4 through a cross-shaped well (in the center), obtained using values of θ_1, θ_2, r_0 that minimize the energy. The first thing to notice is that the energies of the slipped parallel and cross-minima differ by only about 3 cm^{-1}. We therefore expect the cross-structure to play an important role in the dynamics of this complex. The height of the barrier between SP and cross-wells is also small, only about 40 cm^{-1}. This is much smaller than the height of the planar barriers separating isomers. Therefore, a state localized in a SP well would propagate to another SP well along a non-planar path. Finally, there are two symmetrically equivalent cross wells.

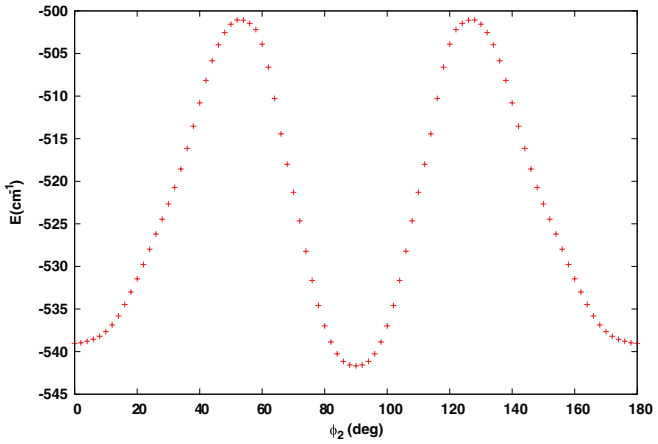

FIG. 4. Torsion profile obtained by minimizing θ_2, θ_2, r_0 while changing ϕ_2. The middle well is a cross-shaped well and the outside wells are SP wells. The barrier top occurs at 53.1° and 126.9°.

IV. CALCULATING ROVIBRATIONAL ENERGIES

The rovibrational Schrödinger equation was solved using the method described in Refs. 14 and 26. Potential terms that couple inter- and intra-monomer coordinates are neglected; only the 4 intermolecular vibrational coordinates are explicitly treated and experimental ground state rotational constants are used for the monomers. The values we use are 0.39021894 cm^{-1} for[45] CO_2 and 0.109159873 cm^{-1} for[46] CS_2. Focusing on only the intermolecular coordinates is commonly justified by arguing that the intramolecular frequencies are much larger than the intermolecular frequencies. The four vibrational coordinates are θ_1, θ_2, ϕ_2, r_0. They are defined in Sec. II. The three rotational coordinates are Euler angles specifying the orientation of a body-fixed frame attached such that the z-axis is along $\vec{r}_0$ and the x-axis is along the vector $(\vec{r}_0 \times \vec{r}_1) \times \vec{r}_0$. The kinetic energy operator (KEO) is well known.[47,48] The masses used to compute the reduced mass associated with r_0, are 15.9949146221,[49] 12, 31.972071[50] amu for O, C, and S, respectively.

Energy levels and intensities are computed by representing the Hamiltonian in a large product basis and applying the symmetry adapted Lanczos (SAL) algorithm.[51–53] Other iterative approaches have also been used in recent years.[54–57] For the bend and rotational coordinates, we use parity-adapted rovibrational functions[58,59] and calculate states of even and odd parity with different bases. In our calculations, the angular quantum numbers of the bend-rotation functions, l_1, l_2, and m_2, all have the same maximal value, $l_{max} = m_{max} = 52$. Gauss quadrature is used for potential matrix-vector products and sums are evaluated sequentially. KEO matrix elements are exact. Matrix-vector products are done by evaluating sums sequentially.[15,48,60–63] We used 53 Gauss-Legendre quadrature points for θ_1 and θ_2 and 106 trapezoid points in the range $[0, 2\pi]$, with the first point at zero, for ϕ_2. For r_0, we use 25 PODVR (potential-optimized DVR) functions.[5,62,64–66] The reference potential that defines the PODVR functions is a cut potential in the range [5.3 bohr, 20 bohr] with all other coordinates fixed at their equilibrium values in the cross-shaped well. The vibrational even-parity basis size is 1 275 975. Tests with a huge basis, having 200 sine DVR functions[5,62,67] for r_0 and an angular basis with $l_{max} = 52$, confirm that the smaller basis set (with 25 r_0 PODVR functions) converges levels near 50 cm^{-1} above the zero point energy (ZPE) to better than 0.001 cm^{-1}. To reduce the spectral range,[60] we apply a potential ceiling of 2098.0 cm^{-1} just below the ceiling used in the generation of the PES. About half the potential points on the direct product grid are replaced with the ceiling value.

The molecular symmetry group[2] for the Hamiltonian we use is G_8, composed of the feasible operations $\{E, E^*\}\otimes\{E, \sigma_O, \sigma_S, \sigma_{OS}\}$, where σ_{OS} is exchange of both O and S nuclei, σ_O is exchange of the O nuclei, and σ_S is exchange of the S nuclei. There are 8 irreducible representations which we label +ee,+eo,+oe,+oo,−ee,−eo,−oe,−oo. ± label even and odd parities. e/o label states symmetric and antisymmetric with respect to σ_O and σ_S. From the effect of the symmetry operations on the parity-adapted rovibrational basis $u^{JMP}_{l_1 l_2 m_2; K}$, given in Ref. 68, we deduce that symmetry-adapted basis

functions are symmetric (anti-symmetric) with respect to permutation of the S atoms if l_2 is even (odd) and symmetric (anti-symmetric) with respect to permutation of the O atoms if l_1 is even (odd). In a given parity block, different e/o states are computed using the SAL and projection operators.[51,52]

V. RESULTS

A. Energies and labels for J = 0 plus rotational constants from J = 1 of ground states of each low lying minima

Table II lists the lowest $J = 0$ energy levels for each irrep of the CO_2–CS_2 complex. The states are labeled (Type;v_t (torsion), v_S(CS_2 monomer bend), v_O (CO_2 monomer bend), v_r(VdW-stretch)). The type indicates the well(s) over which the wavefunction is localized, C for the cross, and SP for slipped-parallel. States in the cross wells are well localized. Some of the states labeled SP are only partially localized. For low-lying states, it is possible to recognize nodal structure along torsion, CS_2 monomer bend, CO_2 monomer bend, and VdW-stretch coordinates. The v_t, v_S, v_O, v_r labels are determined by using the nodal structure of the wavefunctions. In $(N_2O)_2$ and $(OCS)_2$, there was evident nodal structure along geared and antigeared coordinates.[14,26,27] The nodes of bend vibrations of CO_2–CS_2, are therefore fundamentally different because they occur on lines parallel to the axes of a θ_1, θ_2 plot. Of course, there is coupling, and it is most evident for states in the SP wells where states assigned to v_S or v_O overtones actually involve some motion of both monomers. See, for example, Fig. 6 of the supplementary material.[69] The torsional fundamental associated with the cross well is quite low, about 15 cm^{-1} (compared to ~27 cm^{-1} for the CS_2 bend, ~42 cm^{-1} for the CO_2 bend, and ~46 cm^{-1} for the VdW stretch).

TABLE II. The lowest vibrational levels (in cm^{-1}) of CO_2–CS_2 for each irrep relative to the ZPE of −469.4481 cm^{-1}. The quantum numbers v_t (torsion), v_S (CS_2 bend), v_O (CO_2 bend), v_r (VdW-stretch) are for the four intermolecular modes. e and o indicate whether the bend functions for monomers CO_2 and CS_2 are even or odd. + and − are parity labels.

State	Symmetry	State	Symmetry
0.0000(C;0000)	+ee	0.0000(C;0000)	−oo
8.2490(SP;0000)	+oo	15.2583(C;1000)	−ee
8.2491(SP;0000)	+ee	19.0774(SP;1000)	−oo
8.2492(SP;0000)	+oe	19.0815(SP;1000)	−oe
8.2492(SP;0000)	+eo	19.0820(SP;1000)	−eo
15.2609(C;1000)	+oo	19.0893(SP;1000)	−ee
26.6080(C;0100)	+eo	26.7462(C;0100)	−oe
27.4021	+ee	28.2585(C;2000)	−oo
28.1305(SP;2000)	+oe	31.4998(C)	−eo
28.2826(SP;2000)	+oo	35.0531	−ee
28.5047(SP;2000)	+eo	35.6174	−oe
29.4743	+ee	36.9542	−oo
32.2010(C)	+oe	37.1116	−eo
38.1274	+oo	42.1173	−ee
38.7665(SP;0100)	+eo	43.1326	−oe
38.9780(SP;0100)	+oe	44.3758(C;0010)	−eo
38.9793(SP;0100)	+ee	45.6781(C;0001)	−oo
39.1878(SP;0100)	+oo	48.6765	−oo
39.6959	+eo	50.1900(SP;1100)	−eo
41.9180(C;0010)	+oe	50.2348(SP;1100)	−ee
43.1196	+ee	50.3876(SP;1100)	−oe
45.9489(C;0001)	+ee	50.6592(SP;1100)	−oo
47.3260	+oe	51.6713	−eo
48.3401	+oo	52.9659(C)	−ee
49.0200	+eo	54.9497(C)	−oe
53.9229(C)	+oo		
54.2352(SP;0010)	+ee		
54.3144(SP;0010)	+oe		
54.3236(SP;0010)	+eo		
54.4093(SP;0010)	+oo		
54.6404	+ee		

To reconcile the symmetry of the vibrational states with the assignments made in Table II, it is necessary to understand the symmetry of the vibrational fundamentals. The symmetry of a fundamental is the symmetry of the corresponding vibrational displacement coordinate near the bottom of well. For both the cross-shaped and slipped-parallel isomers, the symmetries of v_t, v_S, v_O, and v_r fundamentals are −ee, +eo, +oe, and +ee, respectively. Take, for example, the $v_t = 1$ state; $\delta\phi_2$ is the vibrational coordinate and its symmetry is −ee,[68] for both isomers. For the $v_S = 1$ state, $\delta\theta_2$ is the vibrational coordinate and its symmetry is +eo,[68] for both isomers. Similarly, the $v_O = 1$ state symmetry is +oe. The $v_r = 1$ state symmetry is +ee because it is invariant under all of the symmetry operations of the G_8 group.

Because there are four symmetrically equivalent planar SP wells and two symmetrically equivalent cross wells, each SP level is split into a quadruplet and each cross level is split into a doublet. The doublet of the cross states has symmetries +ee and −oo. It is unusual that the symmetry of the torsional displacement coordinate $\delta\phi_2$, −ee, is not the same (see Table II) as the symmetry of the upper level of the lowest cross tunneling pair (−oo). The two symmetries are the same for the cross state of OCS dimer,[27] for example. The symmetry of the nodeless component of the tunneling doublet is certainly +ee. When irreps of the symmetry group are nondegenerate, the upper level of lowest tunneling pair of a double well will always be odd with respect to all operations that interconvert the two wells. In this case, E^*, σ_O, σ_S all interconvert. Tunneling among the four SP wells is different. The four wells are interconverted among themselves by σ_O and σ_S. Thus, the quadruplet has symmetries +ee, +eo, +oe, and +oo. A tunneling wavefunction can be anti-symmetric only with respect to σ_O, which corresponds to +oe symmetry; it can be anti-symmetric only with respect to σ_S, which corresponds to +eo symmetry; it can be anti-symmetric with respect to both σ_O and σ_S, which corresponds to +oo symmetry. See the wavefunction of Fig. 7. According to our calculations the tunneling splittings are small. This is partly due to the width and height of the barriers and partly due to the large mass that must be moved during the tunneling processes. The tunneling splittings increase with increasing energies. If there were no coupling to other vibrational modes, the symmetry of the lower component of a tunneling doublet of a cross vibrational state would be equal to the symmetry of the vibrational state, and the symmetry of the higher component would be equal to the product of −oo and the symmetry of the vibrational state. This rule only fails for the (C;0001) state whose vibrational

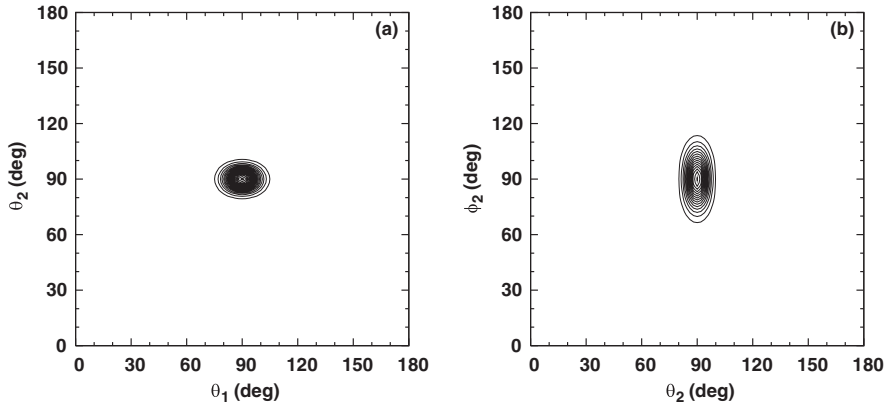

FIG. 5. The (C;0000)(+ee) PD.

energy is high. For many SP states, the +ee state is not the lowest.

As the barrier between SP and cross wells is only 40 cm^{-1}, some states with energies more than 30 cm^{-1} above the ZPE have amplitude in all 4 SP wells and both cross wells, and the labeling of states becomes ambiguous. This is why many of the states in Table II do not have labels for the well. Even some states localized in a well, cannot be assigned an (v_t,v_S,v_O,v_r) label, due to ambiguous nodal structure. Probability density (PD) plots were made by integrating the squared wavefunction over all but two coordinates.[14,26,27] The PDs are normalized with a volume element with a $\sin\theta$ factor for each θ and a r_0^2 factor for r_0. Many low-lying states can clearly be associated with a single well. The +ee (SP;0000) and (C;0000) states are shown in Figs. 5 and 6, respectively. The SP states clearly show amplitude in all four SP wells, while the cross states have amplitude in the two cross wells. The PD plots of the four cross fundamentals, and three SP fundamentals are shown in the supplementary material.[69] The tunneling pairs of the (C;1000) and (C;0100) states look quite similar as can be seen in Figs. 1 and 2 of the supplementary material.[69] All four states are also far enough below the barrier height to be localized in the cross wells.

The energies and wavefunctions of the (C;0010) tunneling pair are quite different. This differs from the (C;1000) and (C;0100) tunneling pairs whose tunneling partners have similar energy and shape. As can be seen from Fig. 3 of the supplementary material,[69] the (C;0010)(+oe) state with energy 41.9180 cm^{-1} has significant amplitude in regions outside the cross wells. The (C;0010)(−eo) state (with energy 44.3758 cm^{-1}), on the other hand, is quite well localized in the cross wells. It is suspected that the (C;0010)(+oe) is different due to coupling with the (+oe) state at 47.3260 cm^{-1}. Surprisingly, the VdW stretch fundamental tunneling pair is similar to the (C;1000) and (C;0100) pairs in that it is also well localized, despite having an energy higher than the barrier between the SP and cross wells. The intermonomer distance must be weakly coupled to the torsion coordinate.

Some of the SP states are well localized: for example, the ground (SP;0000), torsion (SP;1000), and CS_2 monomer bend (SP;0100) states. The PDs of the (+eo) and (+oo) (SP;0100) states are somewhat spread out, but clearly localized in the SP wells and have easily identifiable nodal structure. PD plots for the (SP;1000)(+ee) state are shown in Fig. 5 of the supplementary material.[69] Only three states in Table II are labeled (SP;2000). If there were no coupling there would be four (SP;2000) states. Only one state in Table II is labeled (C;2000). If there were no coupling there would be two (C;2000) states. The unassigned 27.4022 cm^{-1}(+ee) and 29.4743 cm^{-1}(+ee) states could be either a (SP;2000) or a (C;2000) state. They both have the proper parity and approximately the correct energy. However, according to the PD plots, neither has the nodal structure expected for (SP;2000)

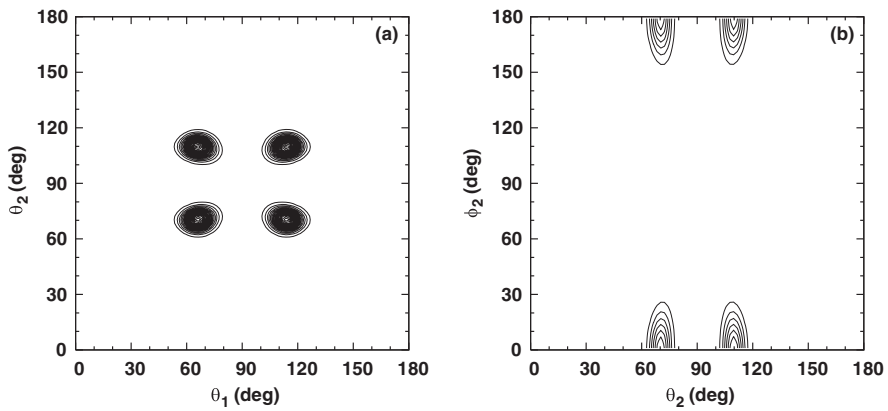

FIG. 6. (a) and (b) The (SP;0000)(+ee) PD. There is amplitude in all four symmetrically equivalent SP wells.

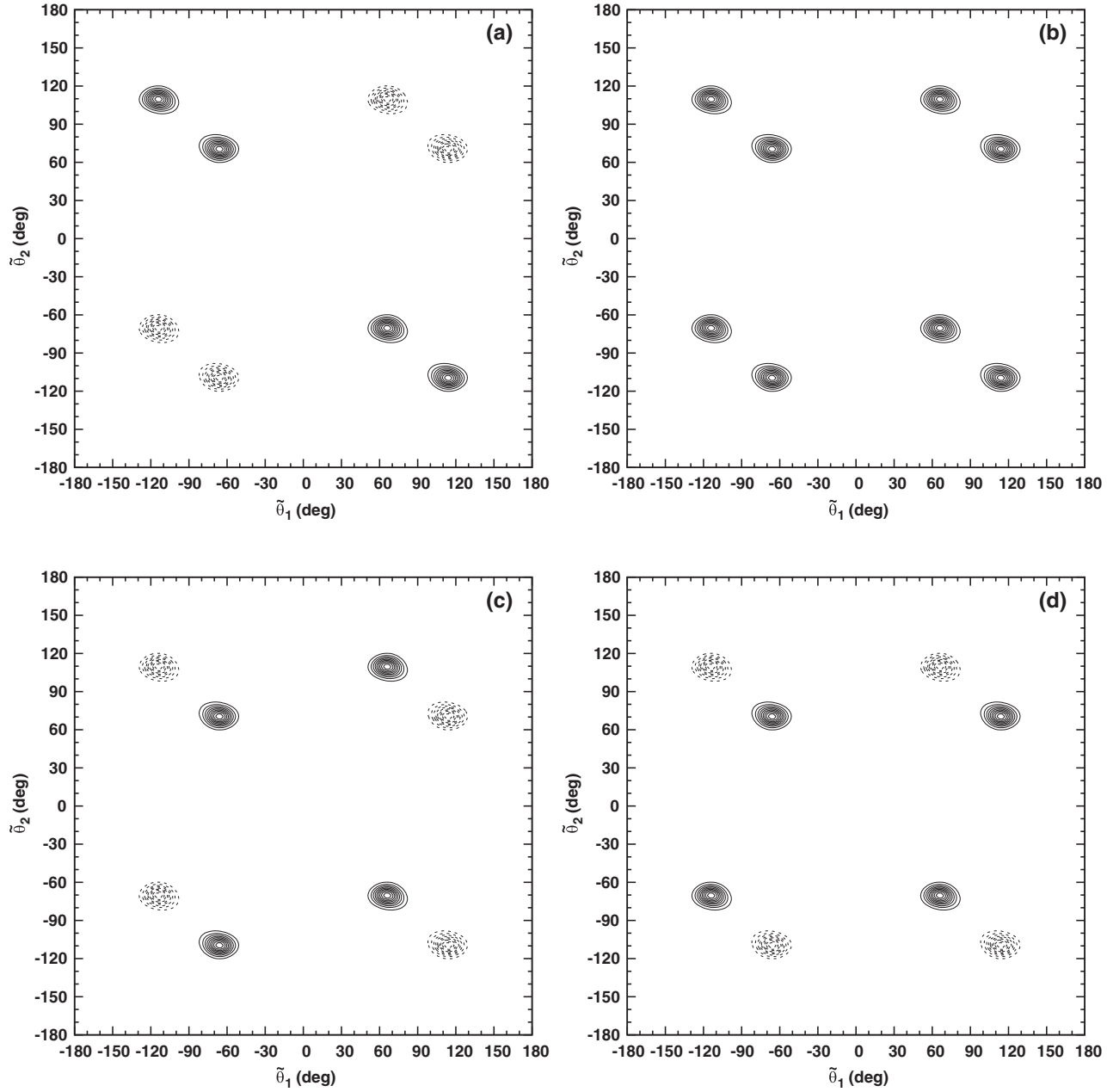

FIG. 7. Wavefunction plot of the quadruplet of the SP ground state at $r_0 = 6.95$ bohr. (a), (b), (c), (d) are the states with energies 8.2490 cm^{-1}(+oo), 8.2492 cm^{-1}(+ee), 8.2492 cm^{-1}(oe+), and 8.2492 cm^{-1}(+eo), respectively The contour interval is 0.2. All four wavefunctions have similar amplitude. For each wavefunction, the amplitude in the four symmetry-related wells is also similar. The first e/o is for $\tilde{\theta}_1$. The sign of the wavefunctions is related to the e/o labels. When $\tilde{\theta}_1 \rightarrow -\tilde{\theta}_1$ the wavefunction does not change sign if the label for θ_1 is e and does change sign if the label for θ_1 is o. This is due to the fact that the operation flips vector $\mathbf{r_1}$. The same applies to the label for θ_2.

and (C;2000). Many of the higher wavefunctions, localized in both SP and C wells, do not have nodal structures that can be easily assigned.

Wavefunctions for the (SP;0000) quadruplet states in extended angles, with r_0 fixed at its equilibrium value, are in Fig. 7. Using extended angles facilitates visualizing large amplitude planar motion without referring to different plots for $\phi_2 = 0$ and π. Thus, the four states appear to be nearly identical and only the PD of the +ee state is shown. The wavefunction plots also provide sign information. The signs in the wells are associated with (eo) labels (see the caption of Fig. 7). The wavefunction plots, however, provide no information for the odd-parity vibrational states because they are zero for planar configurations.

B. $J > 0$ states and rotational constants

Rovibrational levels have also been calculated, and rotational constants compared with experimental results. Dutton *et al.*[35] determined rotational constants by adjusting the constants of an effective rotational Hamiltonian so that its eigenvalues reproduce the rotational energy levels associated with the (C;0000) vibrational state. To do a similar fit for (C;0000)

TABLE III. Comparison of spectroscopic constants of the cross ground state with those of Ref. 35. Constants were obtained from a fit to levels with $J \leq 4$. Values are in cm^{-1}. The bracketed number is one standard deviation in units of the last digit.

Parameter	Ref. 35	This work (+ee)	This work (−oo)
A	0.08590(1)	0.0859080(2)	0.08590787(8)
B	0.04634(1)	0.0464285(2)	0.04642832(5)
C	0.03546(2)	0.0354177(1)	0.03541770(5)
Δ_J	$-1.37(65) \times 10^{-7}$	$1.09(8) \times 10^{-7}$	$1.089(3) \times 10^{-7}$
Δ_{JK}	$-1.01(22) \times 10^{-6}$	$1.03(2) \times 10^{-6}$	$1.014(7) \times 10^{-6}$
Δ_K	$-1.06(23) \times 10^{-6}$	$-1.12(2) \times 10^{-6}$	$-1.108(4) \times 10^{-6}$

and other vibrational states, we must assume that every wavefunction is nearly a product of a vibration/tunneling state, and a rotational state. We must also have a means of assigning vibrational and rotational labels to rovibrational levels. If coupling between rotation and vibration is too strong, this will be impossible. Even when coupling is weak, so that it is possible to associate rovibrational states with vibrational states, it will be difficult to assign rotational labels if the density of vibrational states is high.

Both O and S have zero spin, so only the (±ee) states actually exist. Although this is the case, the (±eo,±oe,±oo) states can still be used to determine rotational constants. There are two (C;0000) states and, by fitting to levels with $J \leq 4$, we have obtained A, B, and C rotational constants and centrifugal distortion constants, Δ_K, Δ_{JK}, and Δ_J.[70] The comparison with experiment is in Table III. The error in the A, B, and C rotational constants is less than 0.0001 cm^{-1}. In Table III, we have changed the sign of the Δ_K reported in Ref. 35 to use the standard definition.[70] The reported experimental and computed Δ_J and Δ_{JK}, constants, have the same magnitude but opposite sign. Negative Δ_J are very rare. Using the SPFIT program[71] we have refit the original data of Ref. 35. The new fitted rotational constants are very close to those of Ref. 35, but the Δ_J and Δ_{JK} constants are both positive: $\Delta_J = 1.7 \times 10^{-7}$ cm^{-1} and $\Delta_{JK} = 8 \times 10^{-7}$ cm^{-1}. A, B, and C rotational constants for the vibrational fundamentals, associated with cross and SP wells, with energy below 50 cm^{-1}, are reported in Table IV. Using the minimum geometry from the PES for the cross-shaped configuration to calculate rigid rotor rotational constants results in A = 0.0849 cm^{-1}, B = 0.0479 cm^{-1}, and C = 0.0363 cm^{-1}. These rotational constants have errors on the order of 0.001 cm^{-1} relative to the experimental results of Ref. 35. The rotational constants presented in Table IV have errors on the order of 0.0001 cm^{-1}. This indicates that accounting for the motion of the nuclei is imperative to achieve excellent agreement with experiment.

To label rovibrational states, we used the vibrational parent analysis (VPA) technique of Refs. 26 and 72. VPA involves expanding the rovibrational wavefunctions in terms of vibrational wavefunctions. To the extent that a rovibrational wavefunction is well described by a product of vibrational (its VP) and rotational functions, it is possible to determine symmetries of rotational functions for each vibrational state. In previous papers, we gave rigid rotor labels (e.g., for $J = 1$, 1_{01}, 1_{11}, 1_{10}) to rotational levels associated with a vibrational state, assuming they were in the same order as they are for a rigid rotor. Then, for each vibrational state, knowing the symmetry of a $J > 0$ state and the symmetry of its vibrational parent and using the product rule, $\Gamma_{vr} = \Gamma_v \Gamma_r$, we determined the symmetry of the rotational factor, Γ_r. In this paper, we use Γ_{vr} to give rigid rotor labels to rotational levels associated with a

TABLE IV. $J = 1$ rotational levels and rotational constants for ground and ν_t, ν_S, ν_O, and ν_r fundamentals of the cross isomer as well as the ground and ν_t and ν_S fundamentals of the SP isomer. Rotational constants are derived from $J = 1$ energy levels.

J = 0(T;v_t,v_g,v_r,v_a)(sym)	1_{01}(sym)	1_{11}(sym)	1_{10}(sym)	A	B	C
0.0000(C;0000)(+ee)	0.0818(−ee)	0.1213(+oe)	0.1323(−oe)	0.0859	0.0464	0.0354
0.0000(C;0000)(−oo)	0.0818(+oo)	0.1213(−eo)	0.1323(+eo)	0.0859	0.0464	0.0354
C_{exp}[35]				0.0859	0.0463	0.0355
15.2609(C;1000)(+oo)	15.3419(−oo)	15.3796(+eo)	15.3907(−eo)	0.0838	0.0461	0.0350
15.2583(C;1000)(−ee)	15.3393(+ee)	15.3816(−oe)	15.3927(+oe)	0.0883	0.0460	0.0350
26.6080(C;0100)(+eo)	26.6879(−eo)	26.8511(+oo)	26.8617(−oo)	0.2085	0.0453	0.0347
26.7462(C;0100)(−oe)	26.8265(+oe)	26.7426(−ee)	26.7543(+ee)	−0.0379	0.0460	0.0343
41.9180(C;0010)(+oe)	41.9965(−oe)	44.4350(+ee)	44.4471(−ee)	2.4838	0.0453	0.0331
44.3758(C;0010)(−eo)	44.4554(+eo)	43.5406(−oo)	43.5488(+oo)	−0.8709	0.0440	0.0357
45.9489(C;0001)(+ee)	46.0287(−ee)	45.7588(+oe)	45.7692(−oe)	−0.2248	0.0451	0.0346
45.6780(C;0001)(−oo)	45.7578(+oo)	46.0929(−eo)	46.1038(+eo)	0.3804	0.0453	0.0345
8.2490(SP;0000)(+oo)	8.3174(−oo)	8.3858(−eo)	8.3964(+eo)	0.1079	0.0395	0.0289
8.2491(SP;0000)(+ee)	8.3175(−ee)	8.3858(−oe)	8.3963(+oe)	0.1078	0.0395	0.0289
8.2492(SP;0000)(+oe)	8.3176(−oe)	8.3859(−ee)	8.3965(+ee)	0.1078	0.0395	0.0289
8.2492(SP;0000)(+eo)	8.3176(−eo)	8.3859(−oo)	8.3965(+oo)	0.1078	0.0395	0.0289
19.0774(SP;1000)(−oo)	19.1470(+oo)	19.2218(+eo)	19.2330(−eo)	0.1152	0.0404	0.0292
19.0815(SP;1000)(−oe)	19.1503(+oe)	19.2173(+ee)	19.2269(−ee)	0.1062	0.0392	0.0296
19.0820(SP;1000)(−eo)	19.1518(+eo)	19.2155(+oo)	19.2265(−oo)	0.1041	0.0404	0.0293
19.0893(SP;1000)(−ee)	19.1575(+ee)	19.2133(+oe)	19.2236(−oe)	0.0950	0.0392	0.0290
38.7665(SP;0100)(+eo)	38.8414(−eo)	39.0998(−oo)	39.1212(+oo)	0.3066	0.0481	0.0268
38.9780(SP;0100)(+oe)	39.0537(−oe)	38.9662(−ee)	38.9892(+ee)	−0.0382	0.0494	0.0264
38.9793(SP;0100)(+ee)	39.0609(−ee)	39.4047(−oe)	39.4197(+oe)	0.3921	0.0483	0.0333
39.1878(SP;0100)(+oo)	39.2668(−oo)	39.1036(−eo)	39.1210(+eo)	−0.1150	0.0482	0.0308

vibrational state (these rotational levels are found via VPA). This is done by using $\Gamma_{vr} = \Gamma_v \Gamma_r$ and the Γ_r established for the ground vibrational state of the appropriate isomer. If coupling between vibration and rotation is small, the two methods of assigning agree. For the cross ground state, the 1_{01}, 1_{11}, 1_{10} rotational functions are −ee, +oe, −oe and for the SP ground state the same rotational functions have symmetries −ee, −oe, +oe.

The new assignment strategy make it possible (see Sec. VI) to fit excited states when we take internal rotation into account.

All of the computed and observed rotational constants for the (C;0000) states are in good agreement. For vibrational states near and above the barrier between SP and cross wells, we attempted to determine rotational constants by fitting parameters of the effective Hamiltonian. Due to the failure of the standard effective Hamiltonian model, caused by rovibrational coupling, this works poorly. When we attempt to fit constants, we find that for two cross states that constitute a tunneling pair, the two *A* rotational constants are not close. The *B* and *C* constants are close. The *A* constant of one member of the tunneling pair is larger than the *A* consistent with the geometry of the cluster; the other *A* is smaller (or even negative!). For states in the SP well, the *B* and *C* constants are all similar, but two of the four tunneling partners have an *A* constant that is much larger, and two have an A constant that is much smaller, than the *A* consistent with the geometry of the cluster. This strange behavior is almost certainly due to internal rotation[73] of the molecule around the *a*-axis, which for the cross states is parallel to the r_0 vector. In Sec. VI, we show that for (C;0100) and (C;1000) cross states, the cross isomer being the only one which is observed experimentally, internal rotation is responsible for the peculiar rovibrational levels.

C. Rovibrational transition line strength

Rovibrational transition line strengths are computed to compare with experiment and to confirm the assignment of rovibrational levels to vibrational parents.[26] Because the two monomers have no permanent dipole, the complex has no microwave transitions when the monomers are frozen. However, if a monomer is stretched asymmetrically, it will have a dipole and a non-zero intramolecular dipole matrix element will make transitions allowed. For this reason infra-red (IR) spectra, such as the IR band observed by Dutton *et al.*[35] near the anti-symmetric ν_3 vibrational frequency of CO_2 of the cross isomer, can be observed. To compare with this experiment, we attach a dipole to CO_2 monomer. Now, the physically allowed bosonic states are +ee and −ee for the ground state $v = 0$ and +oe and −oe for the excited state $v = 1$ (v denotes the intramonomer vibration). Since the dipole is of symmetry −oe, the symmetry selection rules for the transitions are +ee ($v = 0$) → −oe ($v = 1$) and −ee ($v = 0$) → +oe ($v = 1$). For the cross isomer, the *c*-axis is along CO_2 (the *b*-axis is parallel to CS_2 and *a*-axis is along vector $\vec{r}_0$), and therefore *c*-type transitions are expected, i.e., the rigid rotor quantum number selection rule is $\Delta K_a = \pm 1$ and $\Delta K_c = 0$. Table V lists *all* the bright IR $J \leq 1$ transitions from $v = 0$ to $v = 1$ states with their line strengths *S* computed using the expressions given in Ref. 26. The wavefunctions are assumed identical in the $v = 0$ and $v = 1$ states. The frequency of Table V should be added to 2346.5448 cm^{-1}, the band center of the cross ground state observed by Dutton *et al.*,[35] to obtain IR transition frequencies. It is pleasing to see that all the bright transitions satisfy the symmetry selection rule and the rigid rotor quantum number selection rule. The bright transitions for the (C;0000) state are those observed by Dutton *et al.*[35] We also computed line strengths of higher *J* transitions. The line strengths for combination bands (inter-vibrational lines) of the cross isomer are also given in Table V, which may aid experimentalists searching for these bands.[74] In particular, the inter-vibrational lines of Table V, despite having line strengths that are smaller than their intra-vibrational counterparts, would be dominant in an experiment with a jet source because of the low temperature. Intra-vibrational lines derive their line strength from an effective dipole on CO_2. Inter-vibrational lines derive their strength from the coordinate dependence of the CO_2 effective dipole. Intra-vibrational transitions are *c*-type because the effective dipole on CO_2 is along the *c*-axis.[26] The inter-vibrational transitions, from (C;0000) to (C;0010), for example, are *a*-type because only the derivative of the *a*-component of the dipole with respect to θ_1 is non-zero. Obviously similar IR bands also exist near the

TABLE V. Bright infra-red transitions between physically allowed states for CO_2–CS_2 for $J \leq 1$ with a dipole attached to the CO_2 monomer. Line strengths are in units of the dipole attached to the CO_2 monomer.

Lower ($v = 0$)	Upper ($v = 1$)	$J''_{K''_a K''_c} \rightarrow J'_{K'_a K'_c}$	Freq (cm^{-1})	Line strength
		Intra-vibrational lines		
		(C;0000)		
0.0000(+ee)	0.1323(−oe)	$0_{00} \rightarrow 1_{10}$	0.1323	0.97
0.0818(−ee)	0.1213(+oe)	$1_{01} \rightarrow 1_{11}$	0.0395	1.46
		(C;1000)		
15.2583(−ee)	15.3927(+oe)	$0_{00} \rightarrow 1_{10}$	0.1344	0.93
15.3393(+ee)	15.3816(−oe)	$1_{01} \rightarrow 1_{11}$	0.0423	1.39
		(C;0100)		
26.7543(+ee)	26.7462(−oe)	$1_{10} \rightarrow 0_{00}$	−0.0081	0.87
26.7426(−ee)	26.8265(+oe)	$1_{11} \rightarrow 1_{01}$	−0.0839	1.30
		(C;0010)		
44.4471(−ee)	41.9180(+oe)	$1_{10} \rightarrow 0_{00}$	−2.5291	0.42
44.4350(+ee)	41.9965(−oe)	$1_{11} \rightarrow 1_{01}$	−2.4385	0.63
		(C;0001)		
45.9489(+ee)	45.7692(−oe)	$0_{00} \rightarrow 1_{10}$	0.1797	0.75
46.0287(−ee)	45.7588(+oe)	$1_{01} \rightarrow 1_{11}$	0.2699	1.13
		Inter-vibrational lines		
		(C;0000) to vibrational states		
		(C;1000)		
0.0000(+ee)	15.3816(−oe)	$0_{00} \rightarrow 1_{11}$	15.3816	1.9×10^{-2}
0.0818(−ee)	15.3927(+oe)	$1_{01} \rightarrow 1_{10}$	15.3109	2.9×10^{-2}
		(C;0010)		
0.0000(+ee)	41.9965(−oe)	$0_{00} \rightarrow 1_{01}$	41.9965	2.9×10^{-3}
0.0818(−ee)	41.9180(+oe)	$1_{01} \rightarrow 0_{00}$	41.8362	2.9×10^{-3}
		(C;0001)		
0.0000(+ee)	45.7692(−oe)	$0_{00} \rightarrow 1_{10}$	45.7692	1.0×10^{-5}
0.0818(−ee)	45.7588(+oe)	$1_{01} \rightarrow 1_{11}$	45.6769	1.0×10^{-5}

anti-symmetric ν_3 vibration frequency of CS_2. The line strengths for these transitions could also be computed with the same method.

VI. IMPROVING THE EFFECTIVE ROTATIONAL HAMILTONIAN MODEL

Important coupling between vibration and rotation invalidates the use of standard effective rotational Hamiltonians for each vibrational state. For CO_2–CS_2, it seems likely that coupling between the large amplitude torsion coordinate and rotation is responsible. In such cases, a good way to deal with the problem is to treat the large amplitude coordinate and rotation together and to derive an effective large amplitude + rotation (LAR) Hamiltonian for each state of the Hamiltonian for the $3N - 7$ (assumed) small amplitude vibrations (SAV).[4,70,73,75,76]

The full Hamiltonian is written as

$$H = H_{LAR}(\alpha, \beta, \gamma, \phi_2) + H_{SAV}(r_0, \theta_1, \theta_2) + H_C(\alpha, \beta, \gamma, \phi_2, r_0, \theta_1, \theta_2) \quad (1)$$

and perturbation theory is used to treat coupling between blocks labeled by quantum numbers for H_{SAV} and thereby obtain effective Hamiltonians for the large amplitude + rotation coordinates. (α, β, γ) are the Euler rotational coordinates. $H_{LAR} = H_r + K_{\phi_2} + V_{\phi_2} + K_{couple}$ contains a rotational KEO, a KEO for ϕ_2, a potential for ϕ_2, and coupling between ϕ_2 and rotation. H_C couples the SAV and LAR coordinates. We assume that if coupling between torsion and rotation about the molecule-fixed z-axis is the most important, the eigenvalues of each LAR effective Hamiltonian can be written as

$$E(J, K_a, K_c, n) = E_{rot}(J, K_a, K_c) + S_n(K_a) + E_{SAV}, \quad (2)$$

where $S_n(K_a)$ is a correction, which accounts for torsion and coupling between torsion and rotation, $E_{rot}(J, K_a, K_c)$ is the energy of the standard effective asymmetric top Hamiltonian[77] H_{rot}, and $n = (v_t, W, p)$ is a composite label with v_t being a torsion label, W being the well label and p labeling a member of a tunneling doublet. E_{SAV} is the vibrational energy of the SAV state. The PD plot of the torsion fundamental (PD plot in Fig. 1 of the supplementary material[69]) shows little coupling between ϕ_2 and other coordinates and therefore supports the idea that coupling between ϕ_2 and rotation is most important. Our goal is to find $S_n(K_a)$, for each SAV state, and to show that with this $S_n(K_a)$, it is possible to choose rotational constants that yield a good fit and are physically reasonable. Perhaps, the same fitting equation could be used to help experimentalists, observing cross states.[74,78]

First, we need to justify the use of Eq. (2). According to Table IV, when a standard fitting Hamiltonian is used, it is only the A constant that is unphysical (not consistent with the shape of the molecule at the bottom of the potential well). This implies that it should indeed be possible to find a correction $S_n(K_a)$. This is confirmed by showing that differences between eigenvalues of the standard rigid rotor Hamiltonian and energy levels computed as explained in Sec. IV (hereafter denoted the full calculation) are nearly equal for states with a given K_a. See Table VI, where numbers in the second and third columns are obtained by subtracting the vibrational energies from the rovibrational energies. The rotational constants used to make Table VI are chosen as follows. B and C are obtained from the frequencies of the $1_{01} \rightarrow 0_{00}$ and $2_{11} \rightarrow 1_{10}$ transitions. For a rigid rotor, the levels labeled by 0_{00}, 1_{01} 1_{10}, and 2_{11} are 0, B+C, A+B, and A+4B+C, respectively. From two energy level differences one obtains a 2×2 system of equations,

$$\begin{pmatrix} 1 & 1 \\ 3 & 1 \end{pmatrix} \begin{bmatrix} B \\ C \end{bmatrix} = \begin{bmatrix} 1_{01} - 0_{00} \\ 2_{11} - 1_{10} \end{bmatrix} \quad (3)$$

which yields values for B and C. The rotational constant A was chosen to minimize the $E_{actual} - E_{ideal}$ difference in the $K_a = 0$ energies. E_{actual} is a computed energy from which the vibrational energy has been subtracted. E_{ideal} is the corresponding rigid rotor energy. Clearly, the differences depend on K_a. This confirms the idea that a K_a dependent correction should be added to the energy level expression used to fit. Similar results are obtained for any reasonable choice of A.

TABLE VI. Differences between the ideal rotational (i.e., rigid rotor) and the actual *ab initio* energies.

	$E_{actual} - E_{ideal}$	
$J_{K_a K_c}$	(C;1000)(+oo)	(C;1000)(−ee)
0_{00}	0.000000	0.000000
1_{01}	0.000000	0.000000
2_{02}	0.000002	0.000002
3_{03}	0.000006	0.000005
4_{04}	−0.000003	−0.000006
1_{11}	0.002267	−0.001850
1_{10}	0.002272	−0.001829
2_{12}	0.002259	−0.001891
2_{11}	0.002272	−0.001829
3_{13}	0.002235	−0.001946
3_{12}	0.002255	−0.001820
4_{14}	0.002184	−0.002015
4_{13}	0.002196	−0.001786
2_{21}	0.000938	0.000762
2_{20}	0.000933	0.000758
3_{22}	0.000876	0.000685
3_{21}	0.000858	0.000669
4_{23}	0.000782	0.000577
4_{22}	0.000749	0.000550
3_{31}	0.000643	0.003126
3_{30}	0.000645	0.003121
4_{32}	0.000456	0.002899
4_{31}	0.000475	0.002864
4_{41}	0.002086	0.004519
4_{40}	0.002086	0.004519

The use of Eq. (2) is also consistent with the idea of a LAR effective Hamiltonian for each SAV vibrational state. We assume that the effective Hamiltonian can be written as

$$H_{LAR}^{eff} = H_{rot} + [H^{model}(a_2, a_4) - A_{comp} J_z^2] + E_{SAV}, \quad (4)$$

where $A_{comp} = \frac{B_{CO_2} B_{CS_2}}{B_{CO_2} + B_{CS_2}}$, H_{rot} is a standard effective rotational Hamiltonian, $H^{model}(a_2, a_4)$ is a 2D model Hamiltonian that depends on the Euler angle for rotation about

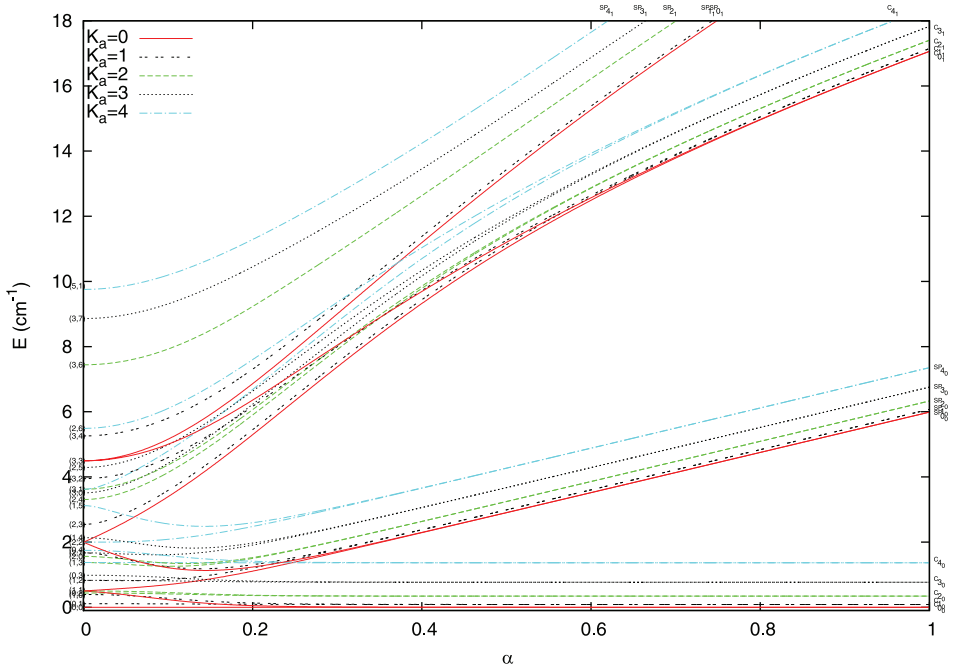

FIG. 8. Correlation diagram of energy vs α. Energies are computed with a model potential which is $\alpha(-3.179\cos(2\phi_2) - 22.485\cos(4\phi_2))$. Therefore, $\alpha = 0$ is the free rotor limit and $\alpha = 1$ is the model potential with the fitted parameters for (C;1000), which is close to the rigid rotor limit.

the molecule-fixed z-axis, ϕ_2, and a_2 and a_4, parameters that determine the height of the torsion barrier. It includes all coupling between rotation and torsion. $H^{model}(a_2, a_4)$ was used in Ref. 79 to study CO_2–C_2H_4. $A_{comp}J_z^2$ is subtracted because rotation is included in H_{rot}. The eigenvalues of H_{LAR}^{eff} can be written $E_{rot}(J, K_a, K_c) + C_n(J, K_a, K_c) + E_{SAV}$. If the complex is nearly a symmetric top, then H_{rot} and $[H^{model}(a_2, a_4) - A_{comp}J_z^2]$ will nearly commute and $C_n(J, K_a, K_c)$ will be close to the eigenvalues of $[H^{model}(a_2, a_4) - A_{comp}J_z^2]$. In this article, we shall set $S_n(K_a)$ equal to eigenvalues of $[H^{model}(a_2, a_4) - A_{comp}J_z^2]$.

A. 2D model Hamiltonian

Rather than writing $H^{model}(a_2, a_4)$ in terms of an Euler angle and ϕ_2, it is simpler to use two ϕ angles,

$$\hat{H}^{model} = B_{CO_2}\hat{M}^2_{CO_2}(\phi_{CO_2}) + B_{CS_2}\hat{M}^2_{CS_2}(\phi_{CS_2}) + \hat{V}(\phi_2), \quad (5)$$

where the $\hat{M}$s are one-dimensional angular momentum operators corresponding to the rotation of the two monomers. The $\hat{M}$ involve derivatives with respect to two monomer ϕ angles that are defined with respect to a spaced-fixed axis system and $\phi_2 = \phi_{CO_2} - \phi_{CS_2}$. $\hat{V}(\phi_2)$ is the torsion potential, which for simplicity is taken as $\hat{V}(\phi_2) = a_2\cos(2\phi_2) + a_4\cos(4\phi_2)$. If only the first term is included, the potential has two planar wells at 0 and π in $[0, 2\pi]$, assuming $a_2 < 0$. If only the second term is included, the potential has two planar and two cross wells at 0, $\pi/2$, π, $3\pi/2$ in $[0, 2\pi]$, assuming $a_4 < 0$. Including both terms gives a potential with two cross wells at $\pi/2$ and $3\pi/2$ and two planar wells at 0 and π. In the $[0, \pi]$ range, the wells and barriers of $\hat{V}(\phi_2)$ are much like those of Fig. 4. The barrier height between a cross well and a SP well is $-2a_4 - (1/8)a_2^2/a_4 + a_2$ relative to the bottom of the cross well at $\phi_2 = \pi/2$ and $-2a_4 - (1/8)a_2^2/a_4 - a_2$ relative to the bottom of the SP wells at $\phi_2 = 0$ and π. The top of the barrier is at $\phi_2 = (1/2)\cos^{-1}(-a_2/(4a_4))$ in $[0, \pi/2]$. $a_4 \neq 0$ is required to make two bumps in $[0, \pi]$. $a_4 < 0$ is required for a cross well.

If $a_2 = a_4 = 0$, then the eigenvalues of $\hat{H}^{model}$ are

$$\hat{H}^{model}(a_2 = 0) = B_{CO_2}M^2_{CO_2} + B_{CS_2}M^2_{CS_2}, \quad (6)$$

and the sum of the M quantum numbers is the total angular momentum about the internal rotation axis. If $a_2 \neq 0$ or $a_4 \neq 0$, the rotors are coupled and the complex becomes nearly rigid if a_2 or a_4 is large. When one (or both) is (are) large, the complex becomes rigid and the eigenvalues are

$$E(K) = A_{comp}K^2 + E_n, \quad (7)$$

where K is the quantum number for the z component of the total angular momentum of the complex, $n = (v_t, W, p)$ is the same composite label used in Eq. (2) with v_t being a torsion label, W being the well label, and p labeling a member of the tunneling doublet.

Eigenvalues of $B_{CO_2}\hat{M}^2_{CO_2}(\phi_{CO_2}) + B_{CS_2}\hat{M}^2_{CS_2}(\phi_{CS_2}) + \alpha(-3.179\cos(2\phi_2) - 22.485\cos(4\phi_2))$ computed using a basis whose functions are products of plane waves are shown in Fig. 8. For the (C;1000) state, the best fit (see below) has $a2 = -3.179$, $a_4 = -22.485$. The free rotor limit is at $\alpha = 0$ and $\alpha = 1$ is the fitted potential values which is close to rigid limit. For clarity, the zero point energy is removed from the model at each a_2, a_4 value. The labels on the left side of Fig. 8, $(|M_{CO_2}|, |M_{CS_2}|)$, are the quantum numbers for the $a_2 = a_4 = 0$ limit. The labels on the right side of Fig. 8, ${}^W K_{a\,v_t}$, are the quantum numbers for the a_2, $a_4 = large$ limit where W is the well C or SP. K_a is either the sum or the difference of M_{CO_2} and M_{CS_2}. If it is a difference, then v_t may be non-zero.

Energy levels with $K_a > 5$ and $v_t > 1$ are omitted from Fig. 8.

To determine the $S_n(K_a)$ correction factors, we need to associate eigenvalues of $H^{model}(a_2, a_4)$ with those of the full calculation. The eigenvalues of the full calculation are labeled by K_a, v_t, W, and p and we therefore need the labels on the right side of Fig. 8. Because we use a plane-wave basis, the levels of $H^{model}(a_2, a_4)$ are easily assigned with the labels on the left. We obtain the labels on the right by following the curves in Fig. 8. For a given E_n, the levels are given by Eq. (7). In the high barrier limit, the energies of two tunneling partners are equal and assigned to the same ${}^W K_{a\,v_t}$ label. In Ref. 79, there is a graph similar to Fig. 8, but no tunneling pairs are evident because one member of the tunneling pair always has an odd M_{CO_2} quantum number and is not Pauli allowed. Note that according to Fig. 8 states for which either M_{CO_2} or M_{CS_2} is odd correlate with ${}^W K_{a\,v_t}$ labels with odd K_a values and in the exact calculation states with odd K_a are always oo or oe or eo and hence forbidden. To assign a p label to each eigenvalue of $H^{model}(a_2, a_4)$, we need only to determine the parity of the wavefunctions. States with odd K are odd and therefore have $p = 1$. States with even K are even and therefore have $p = 0$.

B. Obtaining $S_n(K_a)$ and fitting

It is possible to fit the exact energy levels and to obtain physically reasonable rotational constants by adjusting parameters. In practice, we fit

$$E_{rot}(J, K_a, K_c) + S_n(K_a) - E_n, \tag{8}$$

where E_n is $S_n(K_a = 0)$ with $n = (v_t, W, p = 0)$. The parameters that are adjusted are a_2, a_4, A, B, and C. For the (C;1000) and (C;0100) tunneling pairs with $J \leq 4$, a good fit is obtained. The fit is done by using the conjugate gradient method to minimize the root mean square difference between the exact levels (minus the vibrational energy) and Eq. (8). To ensure that the 2D model eigenvalues are correctly assigned at each step of the minimization, we proceed as follows. First, 2D calculations are done for a small set of (a_2, a_4) points close to the origin. At each point, optimal values of the rotational constants are determined, and the states are given ${}^W K_{a\,v_t}$ labels using a diagram like Fig. 8. Second, at neighboring (a_2, a_4) points the 2D problem is solved, rotational constants are optimized and ${}^W K_{a\,v_t}$ labels are determined by extrapolating the previously determined 2D energies as a function of (a_2, a_4) and assigning the ${}^W K_{a\,v_t}$ label to the state for (a_2, a_4) whose energy nearly coincides with the extrapolated energy for ${}^W K_{a\,v_t}$. After the minimization is complete, we confirm that the assignment is the same as the one obtained by increasing a_2, a_4 to the large barrier limit in small steps.

For the (C;1000) tunneling pair, the best fit to the rovibrational energies obtained with the standard effective Hamiltonian has a root mean square error of 1.27×10^{-2} cm^{-1} for (C;1000)(−ee) and 1.18×10^{-2} cm^{-1} for (C;1000)(+oo). If instead we fit with Eq. (8) the RMSE is 1.5×10^{-3} cm^{-1}, an order of magnitude smaller. The comparison of the two fits is shown in Table VII which shows that the parameters in the fit with $S_n(K_a)$ are much better determined. The distortion constants in column 2 are unphysical because internal rotation is not accounted for. The fitted potential parameters are $a_2 = -3.179$ cm^{-1} and $a_4 = -22.485$ cm^{-1}. A fitted a_4 that is larger than the fitted a_2 is consistent with the potential in Fig. 4 which has minima separated by $\pi/2$.

TABLE VII. Comparison of spectroscopic constants of the (C;1000) state obtained by fitting with the standard effective rotational Hamiltonian (second and third columns) and by fitting with Eq. (8) (fourth column). Constants were obtained from a fit to levels with $J \leq 4$. Values are in cm^{-1}. The bracketed number is one standard deviation in units of the last digit.

Parameter	(C;1000)(+oo)	(C;1000)(−ee)	Fitted (C;1000)
A	0.0859(2)	0.0862(2)	0.086080(10)
B	0.0458(1)	0.0463(1)	0.046045(7)
C	0.0347(1)	0.0352(1)	0.034966(7)
Δ_J	$-8.7(59)\times 10^{-6}$	$8.9(59)\times 10^{-6}$	$2.8(33)\times 10^{-7}$
Δ_{JK}	$-0.4(18)\times 10^{-6}$	$8.(19)\times 10^{-6}$	$2.0(10)\times 10^{-6}$
Δ_K	$1.5(15)\times 10^{-5}$	$-2.0(14)\times 10^{-5}$	$-1.3(8)\times 10^{-6}$

For the (C;0100) tunneling pair, the statistical error of the fit is also reduced by using $S_n(K_a)$, see Table VIII. In this case, we use E_{rot} omitting the centrifugal distortion constants because they cannot be meaningfully determined. For the (C;0100) tunneling pair, the best fit obtained with the standard effective Hamiltonian has a root mean square error of 6.7×10^{-1} cm^{-1} for (C;0100)(+oe) and 6.5×10^{-1} cm^{-1} for (C;0100)(−oe). If instead we fit both partners with Eq. (8), the RMSE is 4.04×10^{-3} cm^{-1}, two orders of magnitude smaller. As shown in Table VIII, the parameters in the fit with $S_n(K_a)$ are much better determined. The fitted potential parameters are $a_2 = -1.120$ cm^{-1} and $a_4 = -0.365$ cm^{-1}. a_2 and a_4 are effective potential parameters and include effects from coordinates not included in the 2D model. Because the (C;0100) tunneling pair involves excitation of the CS_2 bend, the effective potential is different.

For the other cross-shaped states, it is not possible to get a good fit with Eq. (8). This could be because eigenvalues of H^{eff}_{LAR} are not well represented by Eq. (2) or it might be due to coupling between LAR and SAV coordinates. As can be seen in Fig. 3 of the supplementary material,[69] the two (C;0010) states are not well localized in the cross well. As is evident from the VPA, several vibrational states contribute to rovibrational wavefunctions labeled by (C;0010). Our $S_n(K_a)$ correction is based on a model which, for reasonable a_2 and a_4, will have tunneling splittings that are not compatible with the difference between the (C;0010) energies (~ 2.5 cm^{-1}) in

TABLE VIII. Comparison of spectroscopic constants of the (C;0100) state obtained by fitting with the standard effective rotational Hamiltonian (second and third columns) and by fitting with Eq. (8) (fourth column). Constants were obtained from a fit to levels with $J \leq 4$. Values are in cm^{-1}. The bracketed number is one standard deviation in units of the last digit.

Parameter	(C;0100)(+oe)	(C;0100)(−oe)	Fitted (C;0100)
A	0.092(2)	0.079(3)	0.0872(1)
B	0.049(3)	0.039(4)	0.0454(2)
C	0.038(3)	0.031(4)	0.0348(2)

Table III and therefore shifting with $S_n(K_a)$ cannot be expected to work for (C;0010).

Although the $J = 0$ (C;0001) states are well localized, see Fig. 4 of the supplementary material,[69] the corresponding ro-vibrational states are perturbed. This is evident from the VPA of the $K_a = 1$ states. For $K_a = 1$ (C;1000) and (C;0100) ro-vibrational states, the parentage of one $J = 0$ tunneling partner was dominant (greater than 80%). For $K_a = 1$ (C;0001) ro-vibrational states, the dominant parent had a weight less than 80%. For ro-vibrational states associated with (C;0001)(+ee) about 10% could be attributed to an (+ee) state at 43.1196 cm^{-1} and, for ro-vibrational states associated with (C;0001)(−oo) about 10% could be attributed to an (−oo) state at 48.6765 cm^{-1}. Thus, for the (C;0010) and (C;0001) ro-vibrational states coupling invalidates our fitting procedure. For these and many other states, there is no substitute for the full calculations.

VII. CONCLUSION

An accurate PES has been used to calculate a rovibrational spectra of the CO_2–CS_2 VdW complex. The PES was made from CCSD(T)-F12b/VTZ-F12 *ab initio* data and an IMLS interpolation method. Due to both the quality of the *ab initio* calculations and small fitting error, the PES should be excellent. The agreement between experimental and computed rotational constants is also excellent for the ground state. It might now be possible to observe and assign transitions between states localized above the SP wells.

To do the rovibrational calculations, Gauss quadrature is used for the potential, and the sums required to use the Lanczos algorithm to compute energy levels and wavefunctions are evaluated sequentially, obviating the need to calculate and store Hamiltonian matrix elements. The kinetic energy matrix is sparse and non-zero elements are obtained from analytical expressions. Calculations of this kind, with rigid monomers, are not especially difficult, even though the basis size needed can be larger than a million. Obtaining a good PES and analyzing the wavefunctions and energy level patterns is far more difficult. In order to assign $J = 0$ vibrational energy levels, probability distribution plots were made for each of the low-lying energies. Nodal counting was used to assign fundamentals and overtones. The knowledge of fundamental energies was also useful in assigning combination states. For $J > 0$, vibrational parent analyses, which requires expanding the rovibrational states in terms of the vibrational wavefunctions, facilitates making assignments.

Unlike other VdW complexes we have studied, it is not possible to fit rotational states to a standard asymmetric top rotational energy level expression and obtain physically reasonable rotation constants. This is due to important coupling between rotation and (internal) rotation of CO_2 with respect to CS_2 which links two cross-shaped minima over a low barrier. For some states, it is possible to get a good fit, with sensible rotational constants using an effective Hamiltonian that includes rotation and the large amplitude internal rotation. The effective Hamiltonian is based on a 2D model that couples rotation about the inter-monomer axis and internal rotation.

ACKNOWLEDGMENTS

This work was supported by the Canadian Space Agency and the Natural Sciences and Engineering Research Council of Canada. R.D. is supported by the National Science Foundation (CHE-1300945).

[1] J. Tennyson, Comput. Phys. Rep. **4**, 1 (1986).
[2] P. Bunker and P. Jensen, *Molecular Symmetry and Spectroscopy*, 2nd ed. (NRC Research Press, Ottawa, 1998).
[3] G. Brocks, A. van der Avoird, B. Sutcliffe, and J. Tennyson, Mol. Phys. **50**, 1025 (1983).
[4] P. R. Bunker, Annu. Rev. Phys. Chem. **34**, 59 (1983).
[5] Z. Bacic and J. Light, Annu. Rev. Phys. Chem. **40**, 469 (1989).
[6] D. J. Nesbitt, Chem. Rev. **88**, 843 (1988).
[7] J. M. Hutson, Annu. Rev. Phys. Chem. **41**, 123 (1990).
[8] R. C. Cohen and R. J. Saykally, Annu. Rev. Phys. Chem. **42**, 369 (1991).
[9] R. E. Miller, Science **240**, 447 (1988).
[10] D. J. Nesbitt, Annu. Rev. Phys. Chem. **45**, 367 (1994).
[11] R. J. Le Roy and J. S. Carley, "Spectroscopy and potential energy surfaces of van der Waals molecules," *Advances in Chemical Physics* (John Wiley & Sons, Inc., 2007), pp. 353–420.
[12] A. van der Avoird, P. E. S. Wormer, and R. Moszynski, Chem. Rev. **94**, 1931 (1994).
[13] T. Carrington and X.-G. Wang, WIREs: Comput. Mol. Sci. **1**, 952 (2011).
[14] R. Dawes, X.-G. Wang, A. W. Jasper, and T. Carrington, Jr., J. Chem. Phys. **133**, 134304 (2010).
[15] X.-G. Wang, T. Carrington, Jr., J. Tang, and A. R. W. McKellar, J. Chem. Phys. **123**, 034301 (2005).
[16] J. N. Murrell, S. Carter, S. C. Farantos, P. Huxley, and A. J. C. Varandas, *Molecular Potential Energy Surfaces* (Wiley, New York, 1984).
[17] T. Hollebeek, T.-S. Ho, and H. Rabitz, Annu. Rev. Phys. Chem. **50**, 537 (1999).
[18] M. J. T. Jordan, K. C. Thompson, and M. A. Collins, J. Chem. Phys. **102**, 5647 (1995).
[19] M. A. Collins, Theor. Chem. Acc. **108**, 313 (2002).
[20] S. Manzhos and T. Carrington, J. Chem. Phys. **125**, 194105 (2006).
[21] S. Manzhos and T. Carrington, J. Chem. Phys. **127**, 014103 (2007).
[22] B. J. Braams and J. M. Bowman, Int. Rev. Phys. Chem. **28**, 577 (2009).
[23] R. Dawes, D. L. Thompson, A. F. Wagner, and M. Minkoff, J. Chem. Phys. **128**, 084107 (2008).
[24] R. Dawes, A. Passalacqua, A. F. Wagner, T. D. Sewell, M. Minkoff, and D. L. Thompson, J. Chem. Phys. **130**, 144107 (2009).
[25] R. Dawes, A. F. Wagner, and D. L. Thompson, J. Phys. Chem. A **113**, 4709 (2009).
[26] X.-G. Wang, T. Carrington, Jr., R. Dawes, and A. W. Jasper, J. Mol. Spectrosc. **268**, 53 (2011).
[27] J. Brown, X.-G. Wang, R. Dawes, and T. Carrington, Jr., J. Chem. Phys. **136**, 134306 (2012).
[28] M. Aliev and J. Watson, in *Molecular Spectroscopy: Modern Research*, edited by K. N. RAO (Academic Press, 1985), pp. 1–67.
[29] R. S. Altman, M. D. Marshall, and W. Klemperer, J. Chem. Phys. **77**, 4344 (1982).
[30] S. W. Sharpe, Y. P. Zeng, C. Wittig, and R. A. Beaudet, J. Chem. Phys. **92**, 943 (1990).
[31] A. Sazonov and R. A. Beaudet, J. Phys. Chem. A **102**, 2792 (1998).
[32] G. T. Fraser, A. S. Pine, R. D. Suenram, D. C. Dayton, and R. E. Miller, J. Chem. Phys. **90**, 1330 (1989).
[33] D. C. Dayton, L. G. Pedersen, and R. E. Miller, J. Chem. Phys. **93**, 4560 (1990).
[34] K. R. Leopold, G. T. Fraser, and W. Klemperer, J. Chem. Phys. **80**, 1039 (1984).
[35] C. C. Dutton, D. A. Dows, R. Eikey, S. Evans, and R. A. Beaudet, J. Phys. Chem. A **102**, 6904 (1998).
[36] J. Norooz Oliaee, F. Mivehvar, M. Dehghany, and N. Moazzen-Ahmadi, J. Phys. Chem. A **114**, 7311 (2010).
[37] R. E. Bumgarner, D. J. Pauley, and S. G. Kukolich, J. Chem. Phys. **87**, 3749 (1987).
[38] H. D. Osthoff and W. Jäger, Mol. Phys. **104**, 2861 (2006).
[39] R. Dawes, D. L. Thompson, Y. Guo, A. F. Wagner, and M. Minkoff, J. Chem. Phys. **126**, 184108 (2007).
[40] R. Dawes, X.-G. Wang, and T. Carrington, J. Phys. Chem. A **117**, 7612 (2013).

[41]I. M. Sobol, USSR Comput. Math. Math. Phys. **16**, 236 (1976).
[42]H.-J. Werner, P. J. Knowles, G. Knizia, F. R. Manby, M. Schütz, *et al.*, Molpro, version 2012.1, a package of *ab initio* programs, 2012, see http://www.molpro.net.
[43]K. A. Peterson, T. B. Adler, and H.-J. Werner, J. Chem. Phys. **128**, 084102 (2008).
[44]G. M. Berner, A. L. L. East, M. Afshari, M. Dehghany, N. Moazzen-Ahmadi, and A. R. W. McKellar, J. Chem. Phys. **130**, 164305 (2009).
[45]L. S. Rothman and L. D. Young, J. Quant. Spectrosc. Radiat. Transfer **25**, 505 (1981).
[46]D. S. Kummli, H. M. Frey, and S. Leutwyler, J. Chem. Phys. **124**, 144307 (2006).
[47]F. Gatti and C. Iung, Phys. Rep. **484**, 1 (2009).
[48]M. J. Bramley and T. Carrington, Jr., J. Chem. Phys. **99**, 8519 (1993).
[49]G. Audi and A. Wapstra, Nucl. Phys. A **595**, 409 (1995).
[50]G. Audi and A. Wapstra, Nucl. Phys. A **565**, 1 (1993).
[51]X.-G. Wang and T. Carrington, Jr., J. Chem. Phys. **114**, 1473 (2001).
[52]R. Chen and H. Guo, J. Chem. Phys. **114**, 1467 (2001).
[53]X.-G. Wang and T. Carrington, Jr., J. Chem. Phys. **115**, 9781 (2001).
[54]D. Neuhauser, J. Chem. Phys. **93**, 2611 (1990).
[55]R. Lehoucq, S. Gray, D.-H. Zhang, and J. Light, Comput. Phys. Commun. **109**, 15 (1998).
[56]F. Ribeiro, C. Iung, and C. Leforestier, J. Chem. Phys. **123**, 054106 (2005).
[57]S.-W. Huang and T. Carrington, Jr., Chem. Phys. Lett. **312**, 311 (1999).
[58]X.-G. Wang and T. Carrington, Jr., J. Chem. Phys. **118**, 6946 (2003).
[59]X.-G. Wang and T. Carrington, Jr., J. Chem. Phys. **121**, 2937 (2004).
[60]M. J. Bramley, J. W. Tromp, T. Carrington, Jr., and G. C. Corey, J. Chem. Phys. **100**, 6175 (1994).
[61]J. C. Tremblay and T. Carrington, J. Chem. Phys. **125**, 094311 (2006).
[62]J. C. Light and T. Carrington, Jr., "Discrete-variable representations and their utilization," *Advances in Chemical Physics* (John Wiley & Sons, Inc., 2007), pp. 263–310.
[63]C. Leforestier, J. Chem. Phys. **101**, 7357 (1994).
[64]J. C. Light, I. P. Hamilton, and J. V. Lill, J. Chem. Phys. **82**, 1400 (1985).
[65]H. Wei and T. Carrington, Jr., J. Chem. Phys. **97**, 3029 (1992).
[66]J. Echave and D. C. Clary, Chem. Phys. Lett. **190**, 225 (1992).
[67]D. T. Colbert and W. H. Miller, J. Chem. Phys. **96**, 1982 (1992).
[68]X.-G. Wang and T. Carrington, J. Phys. Chem. A **111**, 10220 (2007).
[69]See supplementary material at http://dx.doi.org/10.1063/1.4867792 for the appendixes which include PD plots for the cross and SP fundamentals.
[70]D. Papoušek, J. M. R. Stone, and V. Špirko, J. Mol. Spectrosc. **48**, 17 (1973).
[71]H. M. Pickett, J. Mol. Spectrosc. **148**, 371 (1991).
[72]E. Matyus, C. Fabri, T. Szidarovszky, G. Czako, W. D. Allen, and A. G. Csaszar, J. Chem. Phys. **133**, 034113 (2010).
[73]C. C. Lin and J. D. Swalen, Rev. Mod. Phys. **31**, 841 (1959).
[74]N. Moazzen-Ahmadi and A. R. W. McKellar, private communication, 2013.
[75]J. Hougen, P. Bunker, and J. Johns, J. Mol. Spectrosc. **34**, 136 (1970).
[76]P. Jensen, Comput. Phys. Rep. **1**, 1 (1983).
[77]D. Papousek and R. Aliev, *Molecular Vibrational-rotational Spectra: Theory and Applications of High Resolution Infrared*, Studies in Physical and Theoretical Chemistry Vol. III (Elsevier, 1982).
[78]N. Moazzen-Ahmadi and A. McKellar, Int. Rev. Phys. Chem. **32**, 611 (2013).
[79]R. J. Bemish, P. A. Block, L. G. Pedersen, and R. E. Miller, J. Chem. Phys. **103**, 7788 (1995).